Hindawi
Advances in Civil Engineering
Volume 2019, Article ID 4392506, 12 pages
https://doi.org/10.1155/2019/4392506

Research Article

Developing Smart Measurement Device to Measure Kinetic Friction Coefficients of Bi-Tilt Isolator

Ming-Hsiang Shih[1] **and Wen-Pei Sung**[2]

[1]*Dept. of Civil Engineering, National Chi-Nan University, Pu-Li, Nan-Tou, 545, Taiwan*
[2]*Dept. of Landscape Architecture, Integrated Research Center for Green Living Technologies, National Chin-Yi University of Technology, Taichung 41170, Taiwan*

Correspondence should be addressed to Wen-Pei Sung; wps@ncut.edu.tw

Received 1 October 2018; Revised 14 November 2018; Accepted 22 November 2018; Published 2 January 2019

Academic Editor: Stefano Sorace

A sliding vibration isolation system, affected by a kinetic friction force, provides a flexible or energy dissipation system for a structure. The kinetic friction coefficient of the contact surfaces between the moving parts changes with the relative moving velocity of the two contact surfaces. In this study, a smart measuring device is proposed to measure the kinetic friction coefficients of materials. The Arduino boards Arduino Nano, Arduino MPU-9250, and Arduino SD modules were combined to create this proposed smart device and mounted on three aluminum extrusions constructed as a horizontal platform. Then, varying amounts of steel gaskets were applied to adjust the various slopes for sliding tests. The time history of the acceleration and displacement responses of test object movements in the sliding process were respectively, recorded and detected by this proposed smart measuring device and the digital image correlation method (DIC). Statistical analyses of all test responses were used to derive the relationship of velocity to kinetic friction coefficient. Test and analysis results showed that (1) the relationship of velocity to kinetic friction coefficient for the conditions of mild lubrication and no lubrication displayed a trend of first decreasing and then increasing with increasing speed, respectively and (2) the relationship of velocity to kinetic friction coefficient for the condition of full lubrication revealed that the kinetic friction coefficient decreased with increasing speed. Test results demonstrated that this proposed smart measurement device, which is low in price and easy to assemble, can easily measure the kinetic friction coefficient of a material under various lubrication conditions.

1. Introduction

Strong earthquakes often cause huge structural deformations, resulting in permanent damage or even collapse. Recently, major earthquakes have broken records worldwide. An earthquake with a Richter intensity of 9.0 in Sumatra, Indonesia, triggered the South Asian tsunami, which killed more than 200,000 people. Then, the most violent strong earthquake in history, with a Richter earthquake intensity of 9.0, occurred in the northeastern part of the Pacific Ocean near Japan. This earthquake initiated a severe tsunami of more than 10 meters in height. Massive amounts of seawater poured into coastal areas and destroyed buildings, leaving more than 20,000 people dead or missing. These disasters motivate people to increase the seismic capacity of the buildings in which they live and work. Thus, civil engineers devote large amounts of manpower and material resources to developing seismic technology to enhance the seismic-proof capabilities of buildings. Presently, structural control [1–4] can be divided into three types: passive control (isolation, shock absorption, and energy dissipation [4–8]), active control [9–12], and semi-active control [13–20]. The principle of structural isolation is to provide a flexible interlayer between the superstructure and foundation. Therefore, the natural period of the whole structural system can be prolonged, eventually longer than the dominating period of an earthquake. As a result, the energy of the earthquake, inputted into the superstructure, can be reduced. In the event of an earthquake, the superstructure will just be lightly deformed. One of the structural isolation is the sliding-type isolation, which can dissipate the energy of the earthquake into structure by friction force.

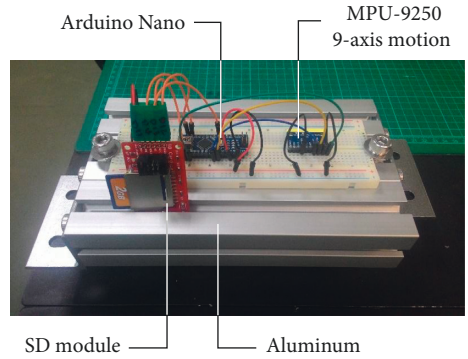

Figure 1: Combined structure of measuring equipment for kinetic friction.

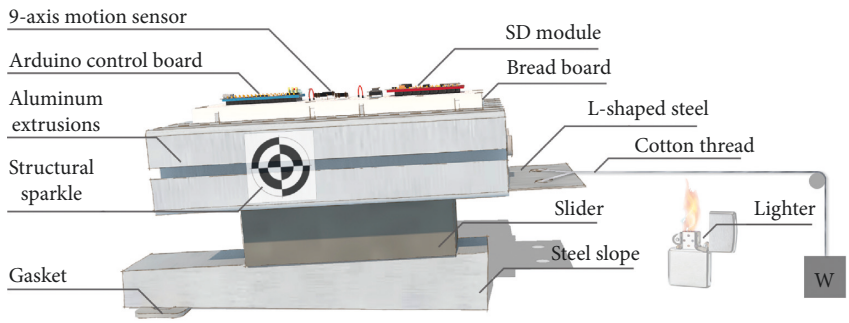

Figure 2: Test setup and the proposed smart measuring device for detecting kinetic friction forces.

The sliding isolation system is evidently affected by frictional force. The coefficient of friction can be divided into static (μs) and kinetic (μd) friction coefficient. The static friction force increases when the action force between the contact surfaces increases. When the action force does not exceed the frictional force, the contact surface remains in static equilibrium. If the action force exceeds the limit of the static friction force, it cannot be increased again, and the contact surfaces begin to slide. The kinetic friction coefficient (μd) is the friction coefficient between two contact surfaces with relative motion and changes with the relative moving velocity of the two contact surfaces; the faster the velocity between two contact surfaces is, the smaller the kinetic friction coefficient is [21]. The kinetic friction coefficient is a variable value, and the static friction coefficient is a constant. Presently, the kinetic friction coefficient is considered a definite value in the process of numerical analysis. However, it is not actually a definite value. The kinetic friction coefficient of a sliding isolation system changes according to the moving velocity in the process of shock absorption. If the kinetic friction coefficient of a sliding isolation system is set as a fixed value, it will affect the precision of the analysis of numerical simulations. On the other hand, kinetic friction force changes with relative velocity. If the kinetic friction coefficient of each sliding isolation pad varies, it will result in unexpected eccentricity of the entire system. This phenomenon greatly affects the safety of a structure with this kind of isolation system. Therefore, a new measuring technique for measuring the real kinetic friction coefficient of a sliding isolation system in the process of shock absorption is proposed in this study.

The bi-tilt isolator (BTI) proposed by Shih and Sung [22] is a new type of sliding-type seismic isolation system for the process of shock absorption. The friction force is affected greatly by the contact surface condition of the BTI of a structure under excitation of earthquake forces. Therefore, to measure the kinetic friction coefficient with different friction conditions of BTI accurately, Arduino boards are applied to develop a smart device for measuring the kinetic friction coefficient, which can be used for numerical simulation of the structural design of a building with a BTI. Then, the actual seismic-proof capability of a building with a BTI can be investigated.

The measurement of the friction coefficient is very complex. The friction coefficient is not only affected by the materials of the contact surfaces and the presence or absence a solid or liquid material separating the contact surfaces; it also varies with the use of different measuring equipment. The coefficient of friction must be measured by a suitable measuring device, as noted by Chang et al. [23]. The appropriate measuring device must have the following characteristics: repeatability, reproducibility, usability, and effectiveness or validity. At present, dozens of types of friction measuring devices have been developed. Commonly used friction measuring devices include the Brungraber Mark II, English XL measuring device, variable incidence tribometer (VIT), horizontal pull slipmeter (HP), portable skid resistance tester (PSRT), and mobile friction measuring device [24, 25]. An inevitable trend in technology, the Arduino board [26], has gained in popularity recently. The Atmel AVR single chip and open-source software and hardware are adopted for Arduino techniques, constructed by an interface of simple I/O open

Figure 3: Camera setup for dynamic test.

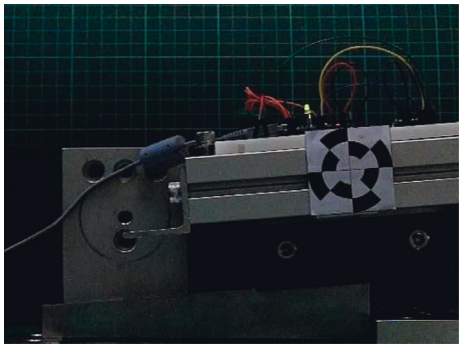

Figure 4: Detected images from dynamic test.

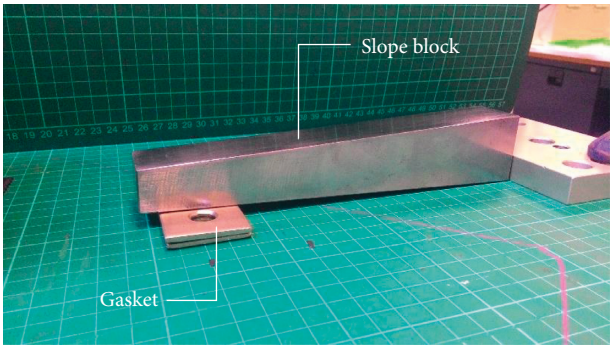

Figure 5: Gasket pad raises slanted steel block to various slope angles.

Table 1: The proportion of a pixel and actual dimensions.

Upper right corner of target	(443, 248)
Lower right corner of target	(435, 152)
Side length of target (pixel)	96.33276
Side length of target (m)	0.05000
The length of one unit pixel (m)	0.00052

Table 2: Initial and stop positions of target coordinates.

Bevel angle (rad)	0.078680	0.111810	0.095126
Target coordinates of initial position	(390, 197)	(366, 201)	(374, 196)
Target coordinate of stop position	(52.15400, 170.75600)	(47.35100, 165.22200)	(46.23000, 164.72600)

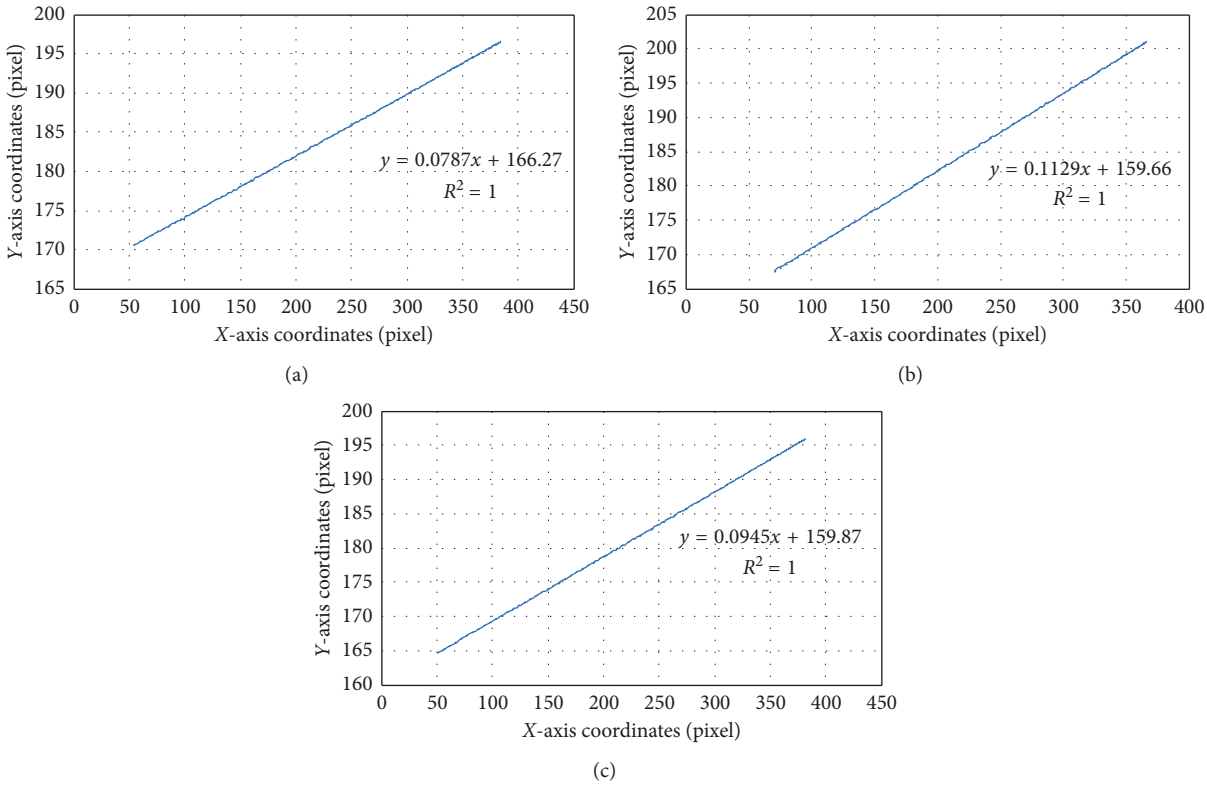

Figure 6: Trend lines of effective slide stages in XY coordinates. (a) Bevel angle 0.0787 rad. (b) Bevel angle 0.1129 rad. (c) Bevel angle 0.0945 rad.

source and using an environment developed in Java or C computer languages. It can be downloaded without charge and modified according to each user's needs. It also can be connected to sensors and other electronic devices [27].

To develop a smart measuring device to measure the kinetic friction coefficient, the Arduino boards (Arduino Nano), motion sensor (MPU-9250), and SD module were applied in this study. The developed device is suitable for a sliding-type isolation system. The acceleration and displacement responses were recorded experimentally with various angles and under different lubrication conditions, and the different kinetic friction coefficients were calculated by a physical mathematical model.

2. Developing Measuring Equipment for Kinetic Friction: Arduino Boards

To develop a simple, accurate, low-cost device that is easy to operate, the widely used technique Maker [26–29] was applied to develop a smart device to detect the kinetic friction coefficients between a friction block and a slanted steel block under various conditions. This developed device is composed of the (1) Arduino Nano, (2) Arduino MPU-9250, and (3) Arduino SD modules mounted on three aluminum extrusions as a horizontal platform, as shown in Figure 1. The Arduino Nano control plate is a small, complete, and bread board-friendly board based on the ATmega328 (Arduino Nano 3.x). It works with a Mini-B USB cable instead of a standard one. Arduino MPU-9250 is a simple example of how to interface the MPU-9250 with the IMU nine degrees of freedom (9DOF)—MPU-9250 breakout board in this Arduino board. The IMU nine degrees of freedom consists of a 3-axis accelerometer, a 3-axis gyroscope, and a 3-axis magnetometer. In this study, a 3-axis accelerometer was used to measure the time history of the acceleration responses of an experimental block with various slope angles. To record all acceleration responses of this experimental block in the sliding process, the Arduino SD module was installed on this proposed block. The electromagnetic compatibility of the Arduino SD module is 5V and 3.3V, so it can be conveniently connected with the Arduino single crystal to process reading and writing of an SD card and also with a power indicator.

3. Experimental Methodology and Calculation

The test setup for detecting the acceleration and displacement responses of a test object in the sliding process for measuring kinetic friction forces is shown in Figure 2.

The accelerometer and the developed dynamic digital image correlation method (DIC) were applied to analyze the acceleration and displacement responses of a test object with various incline angles under various conditions of lubrication. Then, a physical model was applied to calculate the kinetic friction coefficient of the friction block and slanted steel blocks. All test elements of this test setup, shown in Figure 2, are described as follows: (1) test object: aluminum extrusion blocks are combined into a horizontal platform for mounting of the Arduino smart measuring instruments,

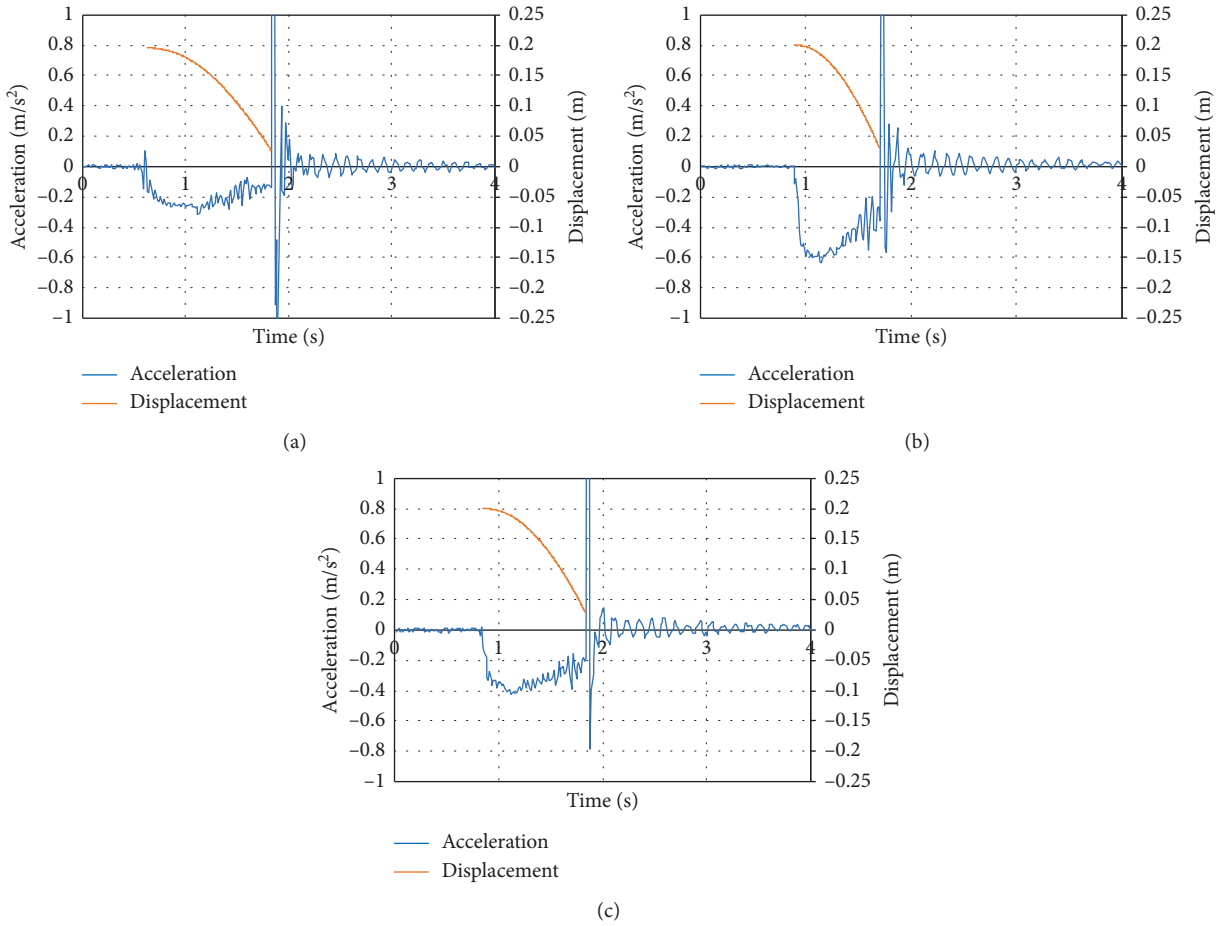

Figure 7: Typical test results of the time history of acceleration and displacement responses. (a) Bevel angle 0.078680 rad. (b) Bevel angle 0.111810 rad. (c) Bevel angle 0.095126 rad.

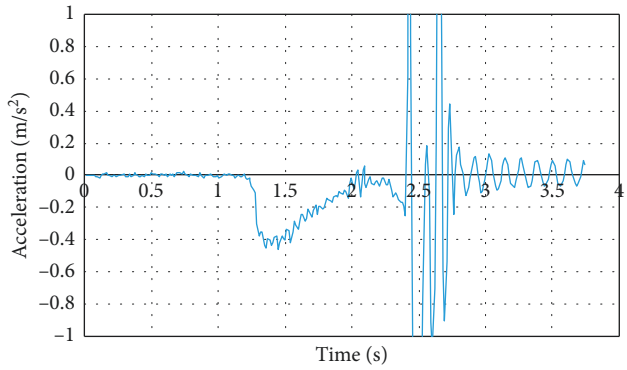

Figure 8: Test results of a typical time history of acceleration responses of counter revolution of the top and bottom ends of the test object with slope angle = 0.095126 rad.

accelerometer, and SD module. Sliding blocks are embedded with friction blocks on the bottom of the block; (2) accelerometer: an accelerometer is glued under the slider block to prevent erroneous signals from the movement process; (3) slanted steel blocks: WD-40 lubricant is applied to the surface of the slanted steel block to simulate different conditions of usage; (4) acceleration and displacement measurement: the gasket is moved to adjust the bevel angle, so the structure does not need to be forced. The surfaces between the friction block and the slanted steel blocks should be smooth for the sliding test.

The test procedure is described as follows: (1) the slider is mounted and the bevel angle is adjusted; (2) the slider is tied with cotton thread fixed to a weight to balance the test setup; (3) the cotton thread is burned at the beginning of the experiment, and the slider begins to slide. This is done to

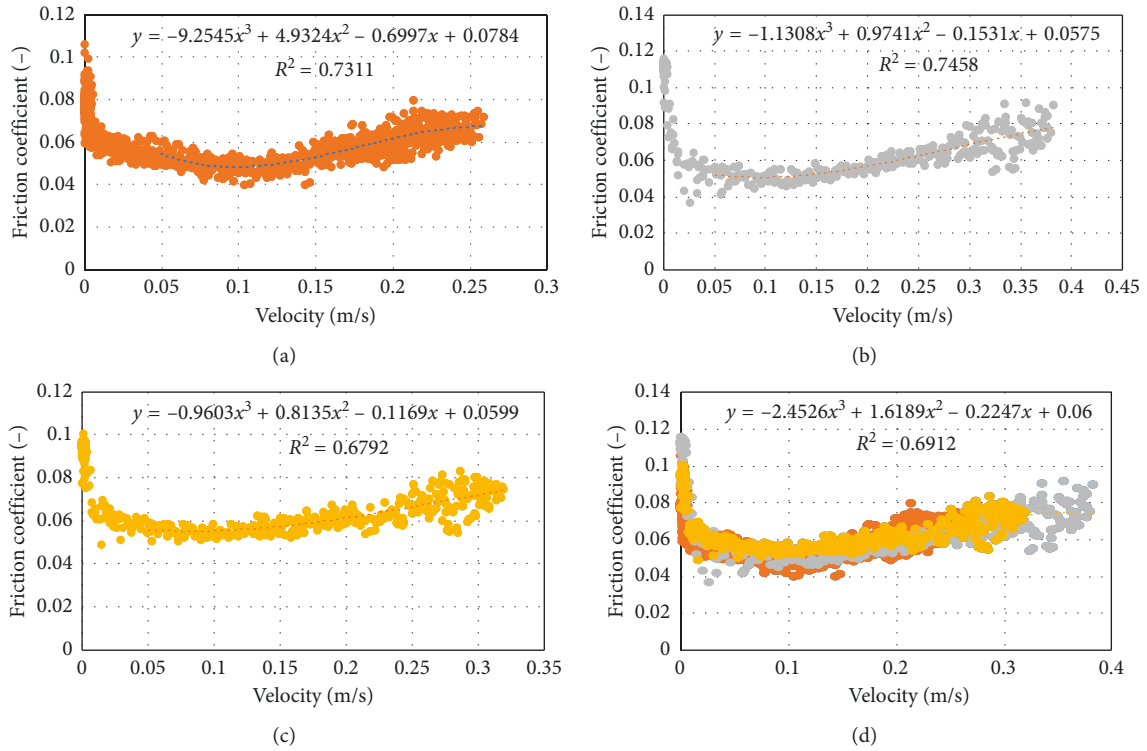

Figure 9: The relationship of speed to kinetic friction before collision. (a) Slope angle = 0.078680 rad. (b) Slope angle = 0.112900 rad. (c) Slope angle = 0.095126 rad. (d) Comparison of test results.

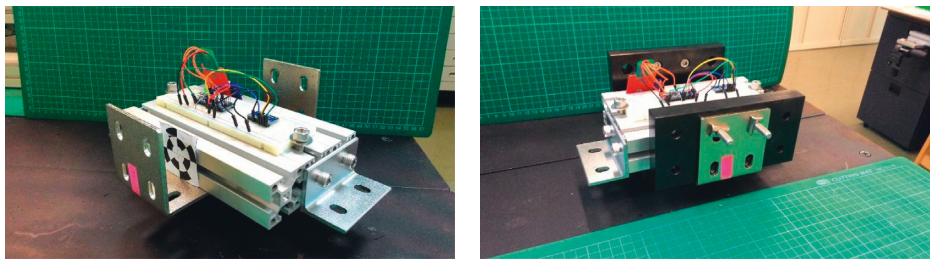

Figure 10: Installation device for testing the influence of normal force on the kinetic friction coefficient. (a) Installed L-shaped steel piece. (b) Mass block installation.

prevent the movement of the slider from being disturbed by the action of being released; (4) the accelerometers on the slider are dropped at the same time, using a frequency of 300 frames per second to record the whole acceleration reaction; (5) simultaneously, the high-speed camera records images of the sliding process to measure the displacement responses.

4. Calculation Method

In this study, the developed dynamic digital image correlation method (DIC) was applied to calculate the angle of the inclined slope. The displacement responses were calculated by the detected images from the structural sparkle on the test object, shown in Figure 2. The calculation method was as follows:

Table 3: Weight of each component.

Component	Weight (kg)
Test object	3.66010
L-shaped steel piece	0.69470
Screws	0.10780
Two mass blocks	3.73690
Four mass blocks	7.47290

$$\theta = \arctan\left(\frac{y_2 - y_1}{x_2 - x_1}\right), \tag{1}$$

where θ is the angle of inclined slope; (x_1, y_1) are the image coordinates of the target before measurement of DIC; and (x_2, y_2) are the image coordinates of the target after measurement of DIC.

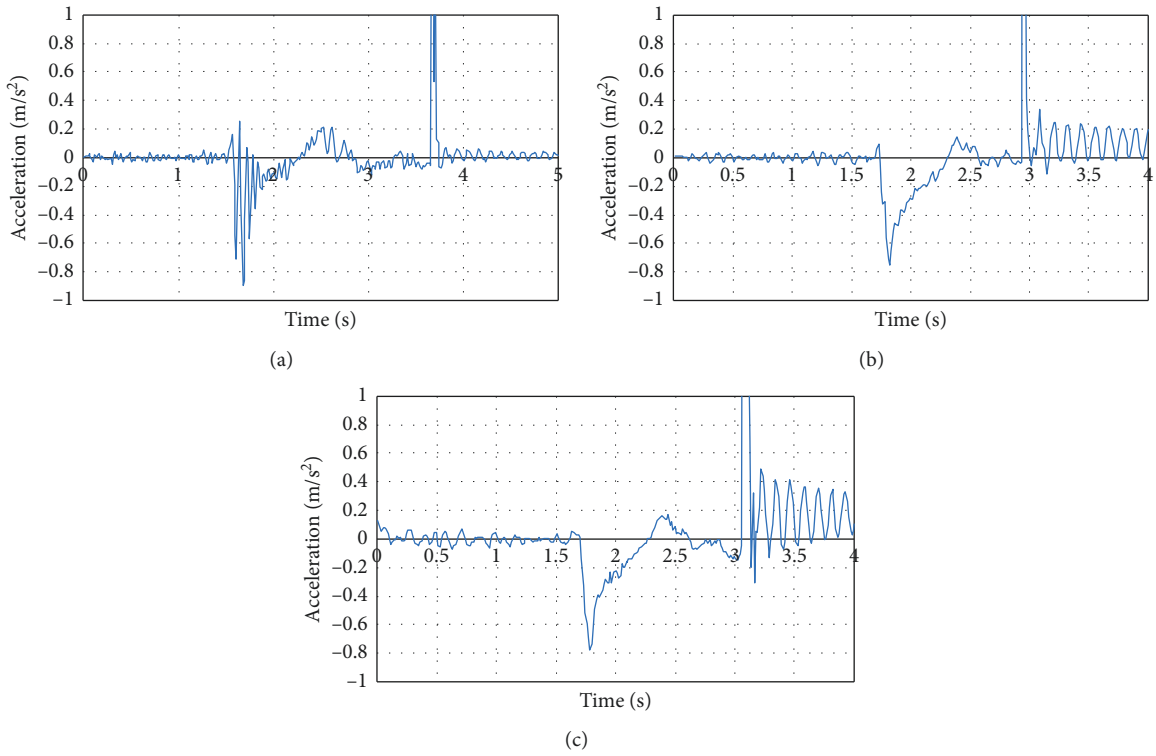

Figure 11: Typical time histories of acceleration responses of the bevel of the steel block under different normal forces (surface cleaned with cleaning naphtha). (a) Normal force = 148, 370 N/m^2. (b) Normal force = 279, 360 N/m^2. (c) Normal force = 406, 650 N/m^2.

Then, the angle θ was used to calculate the descent acceleration of the experimental block. The mathematical model is as follows:

$$a_m = a_s - a_f, \tag{2}$$

where a_m is descent acceleration of experimental block, recorded by the Arduino SD module through the Arduino MPU-9250 and accelerometer; $a_s$is gravity acceleration component along the slope; and $a_f$is acceleration, caused by kinetic friction force.

The gravity acceleration component along the slope was calculated by the following equation:

$$a_s = g \sin \theta, \tag{3}$$

where g is gravity acceleration.

Then, the acceleration caused by the kinetic friction force was calculated by the following equation:

$$a_f = \mu g \cos \theta, \tag{4}$$

where μ is kinetic friction coefficient.

Therefore, the kinetic friction coefficient μ was found by using the above equations with accelerometers, as follows:

$$\mu = \frac{a_m - g \sin \theta}{g \cos \theta}. \tag{5}$$

4.1. Image Recording. The dynamic digital image correlation method was developed by Shih et al. [30, 31]. It is a low-cost method of measuring with high accuracy to detect structural dynamic responses. Therefore, dynamic DIC with high-speed photography was applied to measure all dynamic acceleration in this study.

4.2. Hardware Specifications of Dynamic DIC. The advantage of the DIC method is that the observation points can be set to unlimited. In this study, a high-speed digital camera, the CASIO EXILIM PRO-EX-F1, Figure 3, was employed to record all displacement responses during the experiment. All images were captured by the high-speed image acquisition at 300 frames per second (300 fps). Image specifications were under the 300 fps mode with image resolution of 512 × 384 pixels. Figure 4 shows the black and white mark on the slanted steel block.

4.3. Measurement Procedure. In this study, the dynamic DIC consisted of five procedures to measure the dynamic responses of this test.

Step 1. Set up target: the target should be in the same plane to eliminate proportion differences caused by distance differences. Then, set the proportional ratio scale gage: the constant of proportionality for the image coordinates is obtained with the spatial coordinates by regression analysis.

Step 2. Set up the high-speed camera: the verticality and flattening between the visual axis of the camera and the target plane are tested.

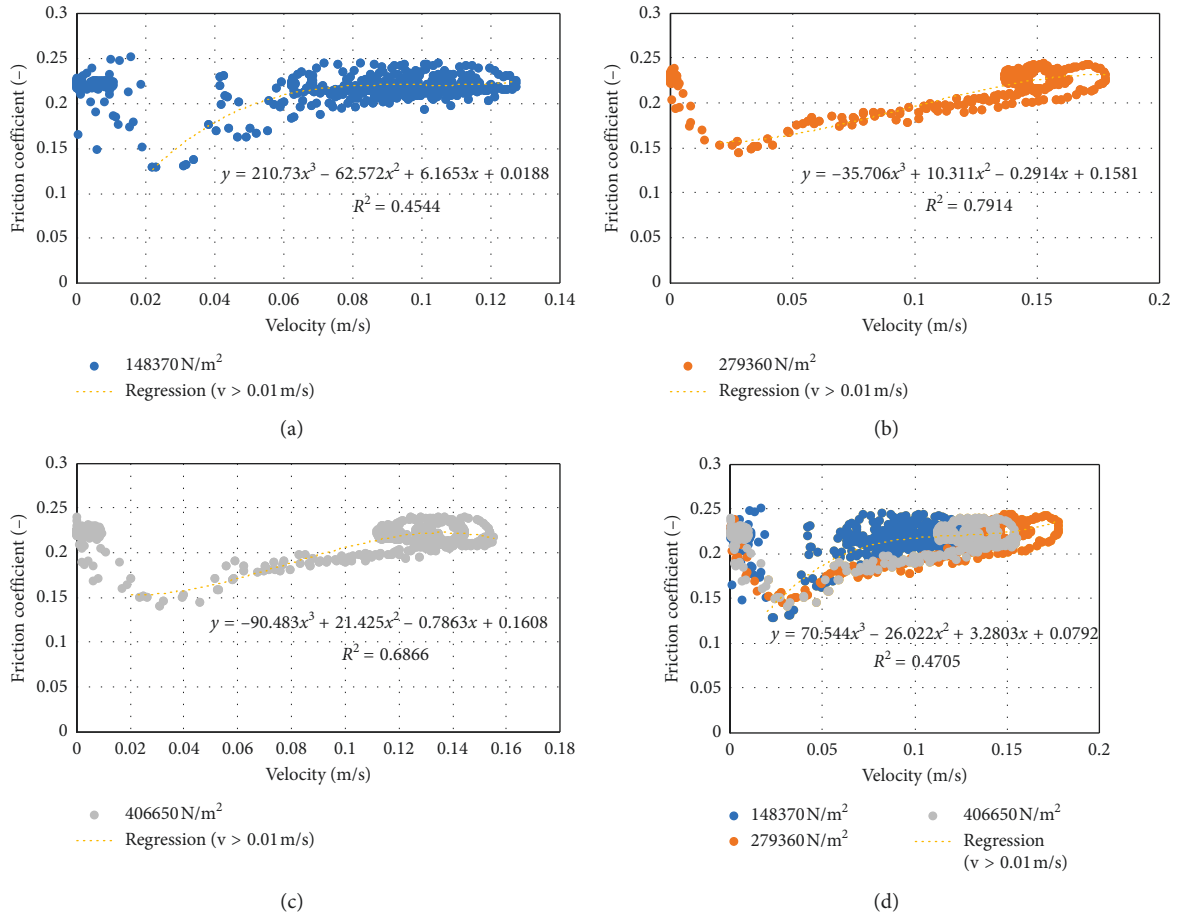

Figure 12: The relationship of speed to the kinetic friction coefficient for the bevel of the steel block with various normal forces (surface cleaned with cleaning naphtha). (a) Average normal force of three test trials = 148, 370 N/m^2. (b) Average normal force of three test trials = 279, 360 N/m^2. (c) Average normal force of three test trials = 406, 650 N/m^2. (d) Comparison of test results of bevel of steel block with different normal forces.

Step 3. Capture dynamic images at 300 fps to ensure a normal exposure value of the shutter within 1/1000 second. For synchronization of the shutter with measurement of the acceleration signals, the program ARDUINO Control is used to control the measurement of the acceleration and to turn on and off the LED lamp. When ARDUINO starts to record the acceleration responses of test object, the LED Lamp will be turned on by ARDUINO Control. Then, the time of the first detected image with light on can be regarded as initial time.

Step 4. Capture dynamic images: the KMPlayer program is applied to capture static and dynamic images.

Step 5. Pair the images from dynamic DIC and spatial coordinate transformation: four subimages are taken as reference images to analyze the center image coordinates of the relative targets of the other images gradually to obtain the time history of the image coordinates for each target from the image center of the target at the start time point.

5. Experimental and Analysis Results and Discussion

5.1. Test Results. To detect the kinetic friction between a friction block and slanted steel blocks with various slopes under different conditions, gasket pads were used at the front and rear ends of the block to form various slopes, as shown in Figure 5. The DIC method was applied to calculate the slope of the block with different conditions. The original slope of the blocks was 0.095126 rad. The other slopes of blocks were 0.078680 and 0.111810 rad, respectively.

The unit of the pixel was recalculated into actual dimensions, as listed in Table 1. The bevel angle was calculated by the target coordinates of the initial and stop positions. The initial and stop positions of the target coordinates and bevel angle are listed in Table 2. The trend lines of the effective slide stages of the test object in XY coordinates, shown in Figure 6, were analyzed to calculate the average bevel angle in ten trials.

Test results of the time history of acceleration and displacement responses are shown in Figure 7. Figures 7(a)–7(c) show the typical test results of ten trials for bevel angles of

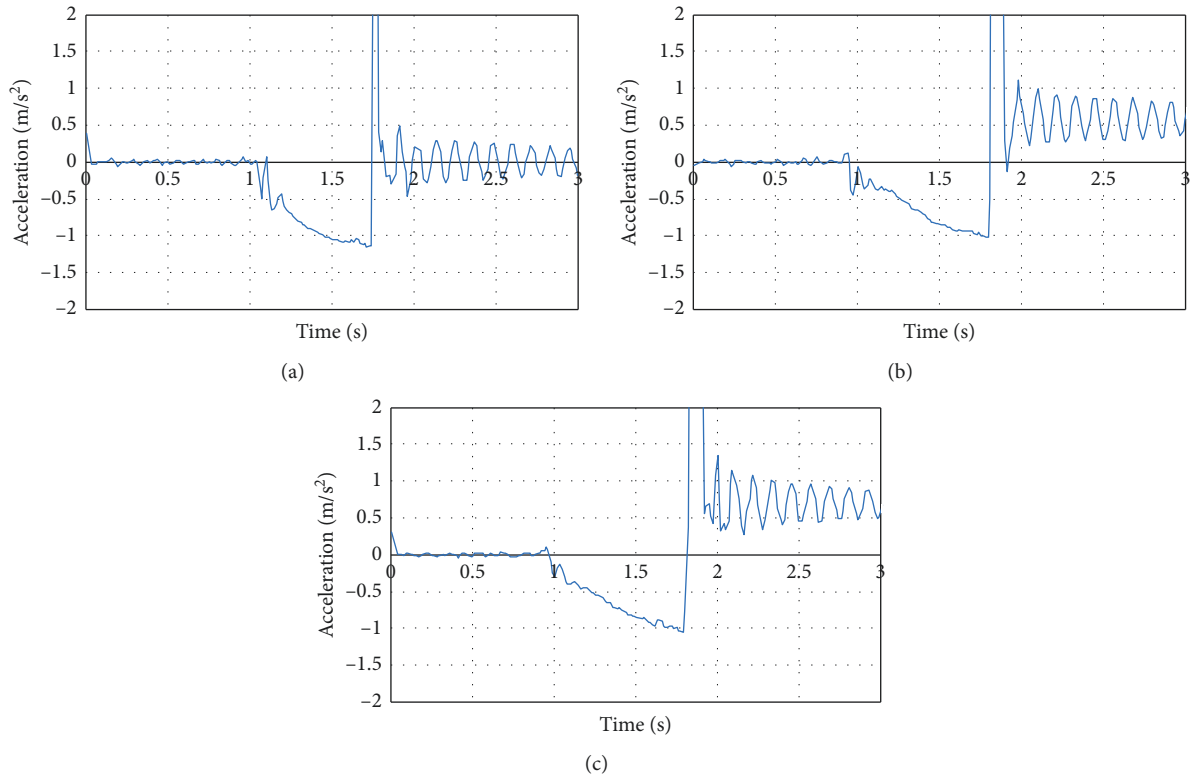

Figure 13: Typical time history of acceleration responses of the bevel of the steel block under different normal forces (surface sprayed with WD-40 lubricating oil). (a) Normal force = 150,040 N/m^2. (b) Normal force = 282,500 N/m^2. (c) Normal force = 411,220 N/m^2.

0.078680, 0.111810, and 0.095126 rad, respectively. The blue and orange lines in Figure 7 represent acceleration and displacement responses, recorded by the accelerometer and MPU-9250, and the analysis results of DIC, respectively. The sliding direction is the axis of the coordinates. The equations in Figure 7 are quadratic regression analysis results of test object displacement responses in the slope moving direction. R^2 of the DIC analysis results in Figure 7 are greater than 0.999800.

Test and analysis results showed that the acceleration trend increased and then decreased as the test object slid. To clarify the reasons for this phenomenon, counter revolution of the top and bottom ends of the test object with a slope angle of 0.095126 rad was used to investigate the roughness of each end of the test object. Typical test results of the time history of the acceleration responses of the counter revolution of the top and bottom ends of the test object with a slope angle of 0.095126 rad are shown in Figure 8.

A comparison of Figures 7 and 8 reveals that regardless of which bevel end of the test object slides from, the variation in the trend of sliding acceleration was almost the same, with acceleration at the rear slide stage decreasing. Thus, this phenomenon was caused by velocity changes resulting in changes to the friction coefficient of the WD-40 applied to the slant of the block. To verify this hypothesis, all test results in Figures 7 and 8 were integrated from the initial stage to the stage just before the collision to acquire the velocity. Then, the relationship of speed to kinetic friction before the collision was investigated for mild lubrication with slope angles of 0.0768, 0.1129, and 0.095126 rad, respectively. As shown in Figure 9, the results of cubic regression analysis for the speed of the three tests were greater than 0.05 m/s, which was used to analyze the effect of speed on the kinetic friction coefficient.

Figure 9 reveals that regardless of the slope angle, kinetic friction first decreased and then increased as the speed increased. This phenomenon is the same as that of Figures 7 and 8. Distribution diagrams of velocity to kinetic friction of the three slope angles were mostly overlapping, as shown in Figure 9(d). The cubic regression analysis curve of speed to kinetic coefficient was $\mu = -2.4526v^3 + 1.6189v^2 - 0.2247v + 0.06$, $R^2 = 0.6912$ for speeds greater than 0.05 m/s.

5.2. Influence of Normal Force on Kinetic Friction Coefficient. To further investigate the influence of normal force on the kinetic friction coefficient, the variation of speed with the kinetic friction coefficient was tested and investigated under varied contact surface stress. L-shaped steel pieces were installed on both sides of the test object to place mass blocks as the applied load; the installation device is shown in Figure 10. In two combinations of these tests, the added external weights were 4.35466 kg, 8.19934 kg, and 11.93536 kg, resulting in three different types of stress, as listed in Table 3. The diameter of the contact surface of the friction block was 0.0189 m, and the normal stresses were 152110 N/m^2, 286410 N/m^2, and 416920 N/m^2, respectively.

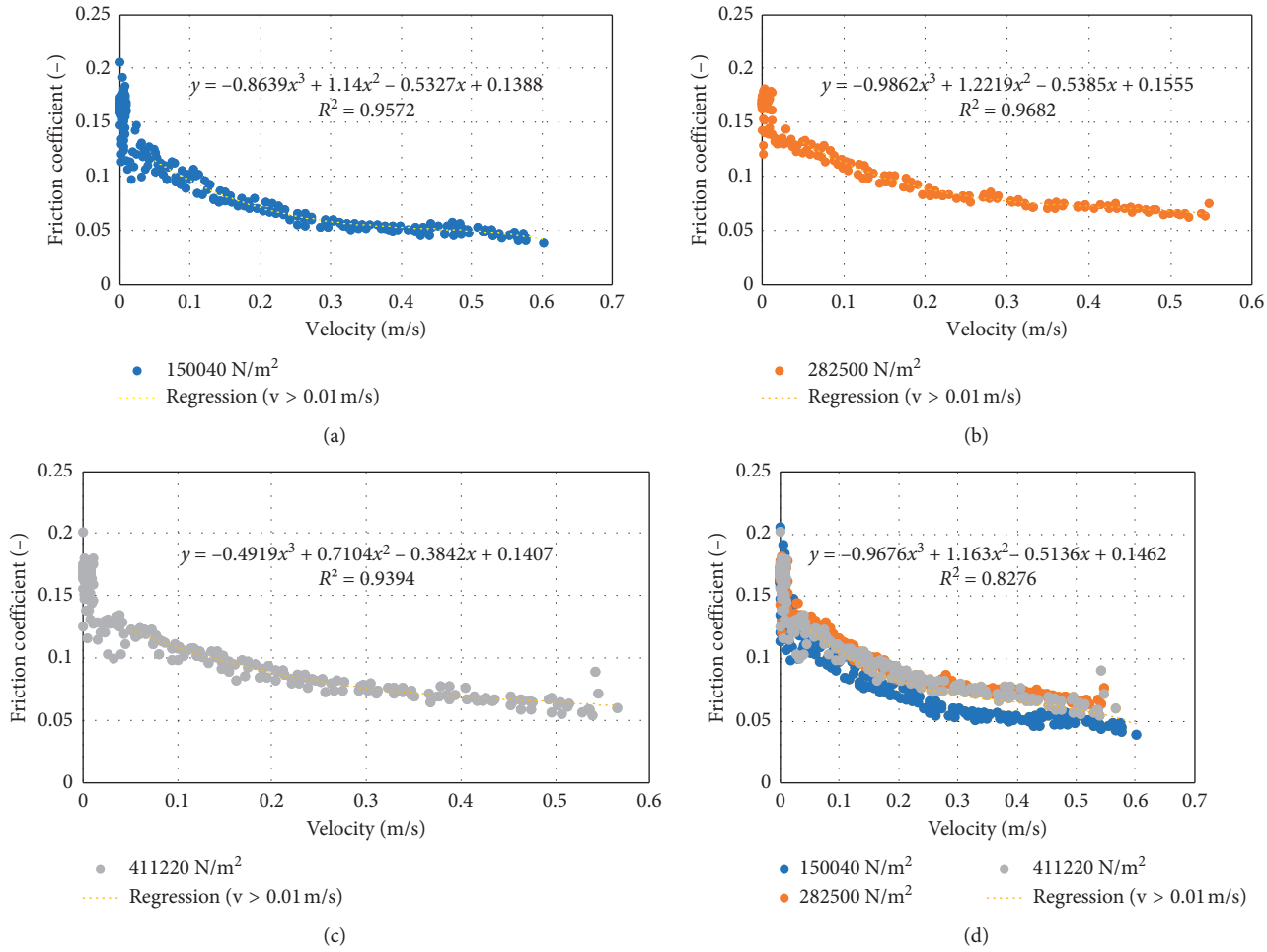

Figure 14: The relationship of speed to the kinetic friction coefficient for the bevel of the steel block under various normal forces (surface sprayed with WD-40 lubricating oil). (a) Average normal force of three test trials = 150, 040 N/m^2. (b) Average normal force of three test trials = 282, 500 N/m^2. (c) Average normal force of three test trials = 411, 220 N/m^2. (d) Comparison of test results of bevel of steel block with different normal forces.

5.3. Test Results. The bevel of the steel block was cleaned with cleaning naphtha to simulate the unlubricated condition, after which three tests were conducted with various normal forces. The experimental angle was changed slightly for each test, and the average angle was about 12.74°. For the time history of acceleration responses, the average acceleration was used as the reference value, as shown in Figure 11, for normal forces of 148, 370 N/m^2, 279, 360 N/m^2, and 406, 650 N/m^2, respectively. Figure 12 is the relationship of speed to kinetic friction coefficient for the bevel of the steel block under different normal forces.

The bevel surface of the steel block was sprayed with WD-40 lubricating oil to simulate the fully lubricated condition, after which three test trials were conducted with various normal forces. The experimental angle changed slightly for each test, and the average angle was about 9.48°. For the time history of acceleration responses, the average acceleration was used as the reference value, as shown in Figure 13, for normal forces of 150, 040 N/m^2, 282, 500 N/m^2, and 411, 220 N/m^2, respectively. Figure 14 presents the relationship of speed to the kinetic friction coefficient for the bevel of the steel block under various normal forces.

Figure 12 reveals that the coefficient of kinetic friction still first decreased and then increased with increasing speed in the case without lubrication. The speed of the test object was slightly lower and then rose in the latter section of the sliding process. The kinetic friction coefficient of this test was around 0.2 to 0.25. The cubic regression curve of the speed was greater than 0.02 m/s, yielding $\mu = 70.544v^3 - 26.022v^2 + 3.2803v + 0.0792$, $R^2 = 0.4705$.

The results in Figure 14 show that the speed of the steel block on the bevel surface sprayed with WD-40 was not yet stable; the test object hit the barrier and stopped sliding. The kinetic friction coefficient decreased with increasing speed until the test object hit the barrier. The cubic regression curve of speed was greater than 0.05 m/s, yielding $\mu = -0.9676v^3 + 1.163v^2 - 0.5136v + 0.1462$, $R^2 = 0.8276$. Whether or not the bevel surface of steel block was sprayed with WD-40, the kinetic friction coefficient changed with changes in speed. The influence of external loading on the kinetic friction coefficient was not obvious.

6. Conclusions

In this study, Arduino boards were applied to develop a smart device for detecting the acceleration responses of a test object in the process of sliding. In addition, a newly developed digital image correlation method was used to detect the displacement responses of the test object while sliding. All these test responses were analyzed statistically to derive the relationship of velocity to the kinetic friction coefficient. The major conclusions of this study are summarized as follows:

(1) All acceleration and displacement responses of this test steel block from start to end can be recorded automatically with this proposed smart device. Moreover, the developed DIC method can detect precisely the position of the test object in the sliding process.

(2) The relationship of sliding velocity to kinetic friction coefficient, shown in Figures 9, 12, and 14, reveals a tendency of variation of the kinetic friction coefficient that is strongly affected by the lubrication condition. The kinetic friction coefficient presents a tendency to decrease first and then to increase as the moving speed of the test object increases under the medium and nonlubricated conditions. In contrast, the kinetic friction coefficient decreases monotonically with the moving speed of the test object under the condition of full lubrication.

(3) The smoother the bevel surface of the steel block is, the faster the speed of the test object is when the kinetic friction coefficient reaches the minimum value. The influences of slope angle and external loading on the kinetic friction coefficient are not obvious.

All test results of this study demonstrate that the Arduino boards Arduino Nano, Arduino MPU-9250, and Arduino SD modules are low-price materials and are easy to assemble into this proposed smart measurement device. This proposed device can easily measure the kinetic friction coefficient of materials under various lubrication conditions.

Data Availability

The data used to support the findings of this study have been deposited in the Experimental Validation of Numerical Model for Bi-Tilt Isolator repository (https://doi.org/10.1155/2018/7163516).

Conflicts of Interest

The authors declare that there are no conflicts of interest regarding the publication of this paper.

Acknowledgments

This research was funded by Ministry of Science and Technology, Taiwan, through grant nos. MOST-104-2625-M-260-001 and MOST-104-2625-M-167-001.

References

[1] G. W. Housner, L. A. Bergman, T. K. Caughey et al., "Structural control: past, present, and future," *Journal of Engineering Mechanics*, vol. 123, no. 9, pp. 897–971, 1997.

[2] J. T. P. Yao, "Concept of structural control," *Journal of the Structural Division*, vol. 1972, pp. 1567–1574, 1972.

[3] B. F. Spencer Jr. and S. Nagarajaiah, "State of the art of structural control," *Journal of Structural Engineering*, vol. 129, no. 7, pp. 845–856, 2003.

[4] L. C. Robert, R. S. Willian, and P. G. Gary, *Adaptive Structures Dynamics & Control*, John Wiley & Sons, Inc., 1998.

[5] S. Iwata, H. Iemura, A. Honda, K. Sakai, T. Fukushima, and K. ugiyama, "Ybrid earthquake loading test (pseudo-dynamic test) of bi-directional base isolation bearing for a large pedestrian bridge," in *Proceedings of 12th World Conference on Earthquake Engineering*, Auckland, New Zealand, 2000.

[6] R. S. Jangid, "Optimum lead-rubber isolation bearings for near-fault motions," *Engineering structures*, vol. 29, no. 10, pp. 2503–2513, 2007.

[7] R. B. Salic, M. A. Garevski, and Z. V. Milutinovic, "Response of lead-rubber bearing isolated structure," in *Proceedings of 14th World Conference on Earthquake Engineering*, Beijing, China, October 2008.

[8] B. Bridget Cunningham, "Using lead rubber bearings in base isolation systems," 2015, https://www.comsol.com/blogs/using-lead-rubber-bearings-in-base-isolation-systems/.

[9] N. R. Fisco and H. Adeli, "Smart structures: Part I-Active and semi-active control," *Scientia Iranica*, vol. 18, no. 3A, pp. 275–284, 2011.

[10] L. L. Chung, R. C. Lin, T. T. Soong, and A. M. Reinhorn, "Experimental study of active control for MDOF seismic structures," *Journal of Engineering Mechanics*, vol. 115, no. 8, pp. 1609–1627, 1989.

[11] K. Liu, L.-X. Chen, and G.-P. Cai, "Active control of a nonlinear and hysteretic building structure with time delay," *Structural Engineering and Mechanics*, vol. 40, no. 3, pp. 431–451, 2011.

[12] X. Zeng, Z. Peng, L. Mo, and G. Y. Su, "Active control based on prediction of structural vibration feedback," *2014 Fifth International Conference on Intelligent Systems Design and Engineering Applications*, , Langkawi, Malaysia, June 2014.

[13] N. Kurata, T. Kobori, M. Takahashi, N. Niwa, and H. Midorikawa, "Actual seismic response controlled building with semi-active damper system," *Earthquake Engineering & Structural Dynamics*, vol. 28, no. 11, pp. 1427–1447, 1999.

[14] F. Palacios-Quiñonero, J. Rubió-Massegú, J. M. Rossell, and H. R. Karimi, "Semiactive-passive structural vibration control strategy for adjacent structures under seismic excitation," *Journal of the Franklin Institute*, vol. 349, no. 10, pp. 3003–3026, 2012.

[15] M. D. Symans and M. C. Constantinou, "Seismic testing of a building structure with a semi-active fluid damper control system," *Earthquake Engineering & Structural Dynamics*, vol. 26, no. 7, pp. 759–777, 1997.

[16] G. J. Hiemenz, Y. T. Choi, and N. M. Wereley, "Seismic control of civil structures utilizing semi-active MR braces," *Computer-Aided Civil and Infrastructure Engineering*, vol. 18, no. 1, pp. 31–44, 2003.

[17] V. Gattulli, M. Lepidi, and F. Potenza, "Seismic protection of frame structures via semi-active control: modeling and implementation issues," *Earthquake Engineering and Engineering Vibration*, vol. 8, no. 4, pp. 627–645, 2010.

[18] N. Caterino, M. Spizzuoco, J. Londoño, and A. Occhiuzzi, "Experimental issues in testing a semiactive technique to control earthquake induced vibration," *Modelling and Simulation in Engineering*, vol. 2014, Article ID 535434, 11 pages, 2014.

[19] S. Pourzeynali and P. Jooei, "Semi-active control of building structures using variable stiffness device and fuzzy logic," *International Journal of Engineering, Transactions A: Basics*, vol. 26, no. 10, pp. 1169–1182, 2013.

[20] K. Hiramoto, T. Matsuoka, and K. Sunakoda, "Simultaneous optimal design of the structural model for the semi-active control design and the model-based semi-active control," *Structural Control and Health Monitoring*, vol. 21, no. 4, pp. 522–541, 2013.

[21] J. Moran and T. Sucharitakul, "Variations in dry sliding friction coefficients with velocity, recent advances on mechanics, materials, mechanical engineering and chemical engineering," in *Proceedings of International Conference on Mechanics, Materials, Mechanical Engineering and Chemical Engineering*, pp. 181–194, Barcelona, Spain, 2015.

[22] M. H. Shih, W. P. Sung, and C. Y. Ho, "Experimental validation of numerical model for Bi-Tilt-Isolator," *Shock and Vibration*, vol. 2018, Article ID 7163516, 12 pages, 2018.

[23] W.-R. Chang, I.-J. Kim, D. P. Manning, and Y. Bunterngchit, "The role of surface roughness in the measurement of slipperiness," *Ergonomics*, vol. 44, pp. 1200–1216, 2010.

[24] http://en.labthink.com/en-us/products/test-property/friction-tester.html?gclid=EAIaIQobChMI07PmiMW53QIVjwMqCh0ZTQvUEAAYAiAAEgK-YPD_BwE.

[25] R. L. Brauer, *Safety and Health for Engineers*, John Wiley & Sons, Inc., Hoboken, NJ, USA, 2nd edition, 2017.

[26] https://learn.sparkfun.com/tutorials/what-is-an-arduino.

[27] https://www.arduino.cc/en/Main/Credits.

[28] https://electronics.stackexchange.com/questions/337496/are-avr-chips-open-source.

[29] https://en.wikipedia.org/wiki/Maker_culture.

[30] M. H. Shih and W. P. Sung, "Developing dynamic digital image correlation technique to monitor structural damage of old buildings under external excitation," *Shock and Vibration*, vol. 2014, Article ID 954840, 15 pages, 2014.

[31] S. H. Tung, M. H. Shih, and W. P. Sung, "Applying the digital-image-correlation technique to measure the deformation of an old building's column retrofitted with steel plate in an in-situ pushover test," *Sadhana*, vol. 39, no. 3, pp. 699–711, 2014.